Adv Syst Sci Appl 2025; **1**; 120-131
Published online at https://ijassa.ipu.ru.

Analysis of Ring Laser Gyroscope Cavity Thermal Deformations

Anton Sinelnikov*

Patrice Lumumba RUDN University, Moscow, Russia

Abstract: Ring laser gyroscopes are crucial for high-precision orientation, stabilization, and autonomous inertial navigation systems. However, their operational accuracy is significantly affected by temperature-induced cavity deformations, leading to potential performance degradation and data loss. This study addresses this challenge by developing a robust algorithm in the MATLAB environment designed to simulate the temperature deformations of a ring laser cavity. Leveraging experimental data, the methodology enables the precise modeling of cavity deformation behavior at various stages of the ring laser gyroscope assembly. The developed mathematical model effectively demonstrates how the addition of structural elements influences the cavity's thermal response and overall deformation. This research provides a novel approach to quantitatively estimate the contribution of individual structural components to the total thermal deformation. The findings offer critical insights for optimizing ring laser gyroscope design, thereby enhancing their accuracy, reliability, and resilience in diverse operational conditions.

Keywords: inertial navigation systems, inertial measurement unit, ring laser gyroscope, cavity, control system, thermal deformations, MATLAB, mathematical model, simulation

1. INTRODUCTION

Due to their high accuracy, reliability and resistance to external influences, ring laser gyroscopes (RLG) are actively used in high-precision systems for orientation, stabilization and navigation [1]. Today, they are employed in aircraft and spacecraft for calculating the angular rotation of a broad range [2].

In the case of inertial navigation guidance, the aerospace vehicles use onboard sensors to determine their motion and acceleration with the help of RLG or other gyroscopes and accelerometers [3]. A gyroscope is used to measure angular rotation, whereas an accelerometer is used to measure linear motion. The two are combined into a single unit along with a control mechanism, and the unit is called inertial measurement unit (IMU), or inertial navigation systems (INS). RLG, is an important optronic rate sensor and, in essence, the heart of any INS [4].

Based on application, RLG market can be split into platform stabilizations as well as aeronautic, missile, submarine and satellite types of navigation [5]. Based on the key end users, RLG commercial market can be divided into business jets, civil aircraft, helicopters and UAVs, general aviation, satellites, spacecraft, and rockets. According to the forecasts, the RLG market volume should exceed $1 billion by 2030 [4,5].

Today optical gyroscopes are one of the dominant technologies in the IMUs and INSs. They are divided into active RLGs and passive Fiber Optical Gyroscopes (FOG) [6]. They uses the Sagnac effect to calculate the rotation rate by measuring the phase shift of two counter propagating light beams in a passive interferometer and frequency difference in an active laser interferometer [7]. According to the Sagnac equation, frequency difference is obtained by fundamental formula (1.1):

* Corresponding author: mr.sinelnikov.a@mail.ru

$$\Delta f = 4S\Omega/\lambda L \quad (1.1)$$

where Δf is the frequency difference between two counter-propagating light waves in the ring laser; S and L are the square and length of the ring laser cavity; Ω is the angular rate; λ is the wavelength of the laser. So, the ideal input-output characteristic of a RLG is described by a simple expression (1.2):

$$\Delta f = K\Omega \quad (1.2)$$

where $K=4S/\lambda L$ is called a scale factor. For a more compact form of this expression a scale factor K is often included into Ω, thereby making the direct relation between the RLG output signal and the measured angular rate more obvious.

Let us consider the analytical review of the Yole Development company to assess the market of inertial navigation systems over the past 10 years [8,9]. The main competitive optical gyroscopes are Hemispherical Resonator Gyroscopes (HRGs), Micro-machined gyros (MEMS) and Dynamically Tuned Gyros (DTGs). Figure 1.1 presents ring diagrams of the evolution of high-end inertial technology market from 2011 to 2019 in monetary value.

As can be seen from the left diagram in Figure 1.1, RLG occupied 40 percent of the inertial systems market in 2011.

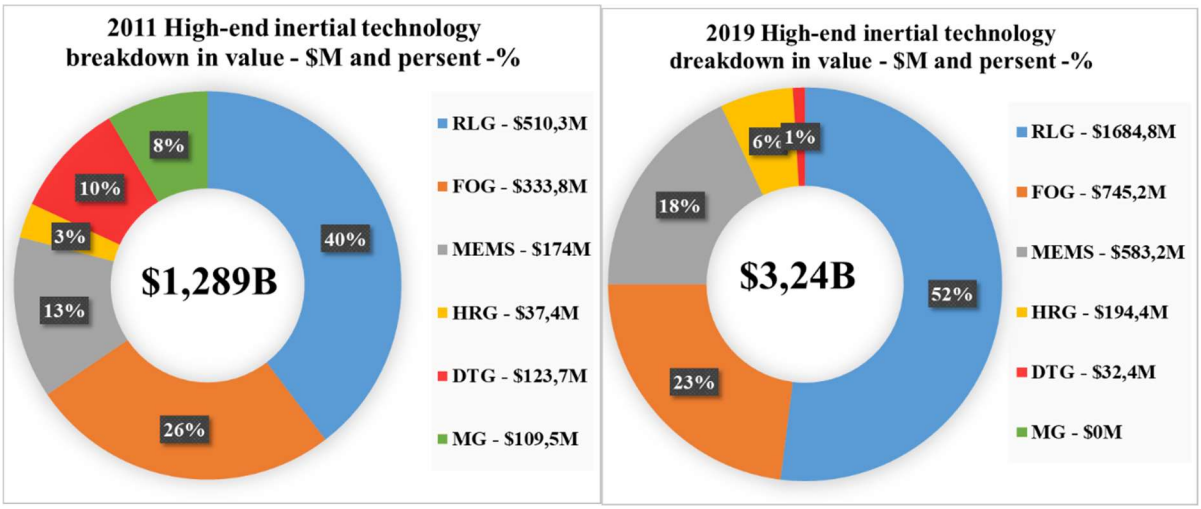

(*a*) (*b*)

Fig. 1.1. Global inertial technology market evolution from 2011 (*a*) to 2019 (*b*) year

It was about $510 million. The entire market was estimated at $1,3 billion. In 2019, the share of RLG increased to 52% as can be seen from the right diagram. This corresponds to $1,7 billion and a threefold increase in a cash volume. The share of FOG decreased by 3 percent, the share of MEMS increased by 5%, the share of HRGs increased by 5%, and the share of other gyros types amounted to 1 percent. So, considering the presented data, RLG technology is dominant in the inertial technology market.

Figure 1.2 shows distribution diagrams of gyroscope types by accuracy class in 2011 and 2019.

It can be seen that MEMS gyros consistently dominate in commercial and industrial navigation. Optical gyros are dominating in tactical navigation. The share of RLG in Midl-term navigation researches 61%. The use of RLG in high-end and strategic navigation is 78%. Give the conservatism of inertial navigation market, the dominance of RLG will continue in the next 10-20 years.

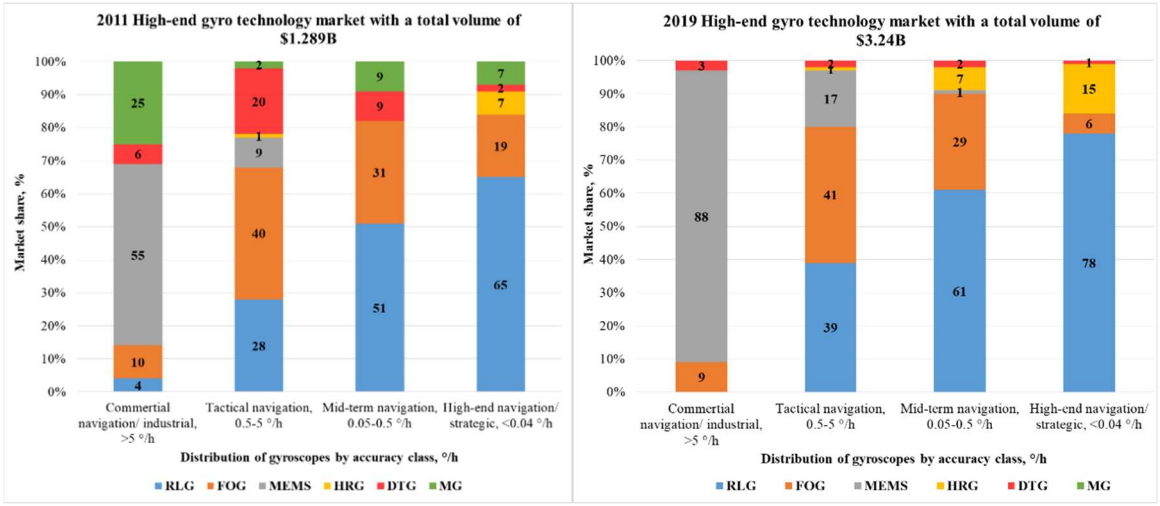

(a) (b)

Fig 1.2. Gyro technology breakdown per bias stability categories from 2011 (a) to 2019 (b) year

There are top-3 types of the most common RLG high-end navigation accuracy class suitable for use in spacecraft among a variety of optical gyroscopes. They are shown in Figure 1.3.

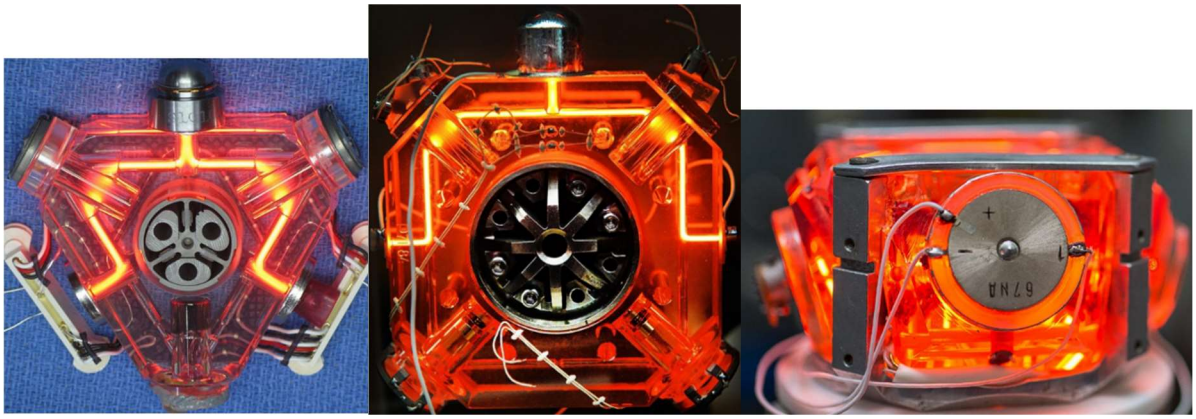

(*a*) (*b*) (*c*)

Fig. 1.3. Most common types of RLG

Commonly used ring laser cavity structure is triangular geometry, as shown in figure 1.3.*a*. This type of geometry is popular with RLGs from Honeywell [10]. Figure 1.3.*b* shows square ring laser geometry, which is one form of geometry in use [11]. These two types of RLG using forced dithering to overcome lock-in effect [12]. Figure 1.3.*c* shows non-polar square-type ring laser geometry that allows the using magneto-optical frequency shift based on Zeeman effect to overcome lock-in effect [13].

Due to the absence of dither, the Zeeman RLG has increased resistance to external mechanical influence [14,15]. This allows using the term in many areas of aerospace industry. However, this may be due to sudden changes in external temperature, which may have a negative impact on the Zeeman RLG operation [16].

The most important condition for achieving all types of RLG stable operation and high precision characteristics, including super-high stability of the scale factor K, is to ensure the constancy of the laser cavity so that the ring laser generates on a single mode [17,18].

The accuracy of timing and stabilizing the laser cavity to keep the generation frequency in the center of the gain curve should be less than a hundredth of die generation wavelength, i.e, units of nanometers ($\lambda\sim$ 1-10nm).

Figure 1.4 illustrates active and passive compensation methods been used to ensure stable operation of the RLG under temperature influences.

(*a*) (*b*)

Fig. 1.4. Active and passive methods for the RLG cavity thermal stabilization

The adjustment of the RLG to the working mode and the time of continuous operation in it is provided by the cavity control system (CCS), which is an active thermal compensation system [18, 19]. At the same time, a wide range of operating temperatures and heating of the Zeeman RLG during its operation impose significant restrictions on the dynamic range of the CCS, therefore, in addition to the active method, a passive method of thermal compensation is used [20]. To provide passive thermal compensation, the gyroscope cavity materials should have ultra-low thermal expansion coefficient (TEC) [21]. This materials include glass ceramics of the brands Zerodur, Clearceram, Cervit and *SO*-115*M* Sitall [22-24].

In particular, the housings of the ring laser cavity and mirror substrates in Russia are made of grade *SO*-115*M* Sitall. The use of this material in the manufacture of RLG structural elements is determined by a number of indisputable advantages, which include an ultra-low TEC, optical transparency and increased retention of the active medium inside the cavity [24]. The main disadvantage of this material is the non-linear nature of the TEC in the range of operating temperatures for measuring systems based on ring laser sensors, which limits the possibility of cavity perimeter active adjustment [25].

In addition to the cavity itself, there are other structural elements in the RLG. These include fasteners, piezoelectric actuators (executive elements of an active CCS), magnetic screens, etc. These structural elements are made of various materials, which have different TEC than glass-ceramic material, which directly affects the temperature stability of the ring laser cavity [26]. To varying degrees, this problem is inherent in all types of modern optical gyroscopes, and mathematical modeling methods are actively used to solve it and temperature correction [27-29].

The purpose of this work is to develop an algorithm in the MATLAB environment, with which it is possible to simulate the Zeeman RLG cavity temperature deformations.

To achieve this goal, the following tasks are solved in the work:

- Obtaining initial data for modeling;
- Development and implementation of the algorithm in the MATLAB environment;
- Development of a temperature drift model for path length of a ring laser cavity.

2. THEORETICAL AND EXPERIMENTAL PART

A sensitive RLG is a *He-Ne* laser with a non-planar optical cavity (Fig. 1.3.*c*) that generates laser beams with circular polarization at a wavelength of λ= 632,8 nm. This makes it possible to use a magneto-optical frequency bias based on the Zeeman effect to remove the RLG from the capture region and form a reference signal for the active CCS. The spectrum of natural

frequencies of longitudinal modes of a non-planar four-mirror cavity Zeeman RLG is half the beams wavelength $\lambda/2$, which corresponds to 316,4 nm [30].

Two movable mirrors of the RLG resonator are equipped with piezoelectric actuators, which ensure the operation of the active CCS [31]. A part of the beam is put out through a semitransparent mirror to the mixing unit to form output signals and obtain information about rotation. The cavity is installed on the base, fixed with special fasteners and placed in magnetic screens. The CCS inputs receive a cavity detuning signal *Ap* from a special photodetector installed in the RLG, and a reference signal synchronous with the current of the alternating frequency bias.

Cavity stabilization is carried out by integrating the signal rectified by a synchronous detector from the photodetector, followed by converting the output voltage of the integrator into a voltage proportional to it on the actuating piezoelectric actuators that move the movable mirrors in the direction of decreasing the error signal. From this it follows that the signal amplitude *Ap* is proportional to the cavity detuning in units of the generation frequency, which in turn is proportional to the temperature deformation of the ring laser cavity.

Setting the path length to the center of the RLG amplification circuit in the open CCS mode corresponds to the minimum value of the cavity signal amplitude, and the detuning corresponds to the maximum.

Thus, in the studied RLG, from the amplitude of the signal *Ap*, it is possible to estimate, with an accuracy of one fourth of the generation wavelength $\lambda/4$ the cavity temperature deformation and its direction from the change in the phase of the signal *Ap*.

To build a model of the RLG cavity thermal deformations, studies of the *ZLK*-16 type device were carried out under long-term temperature effects according to the methodology presented in and obtained the necessary initial data [32]. Figure 2.1 demonstrates a general view of the experimental setup for obtaining initial data for computer modeling.

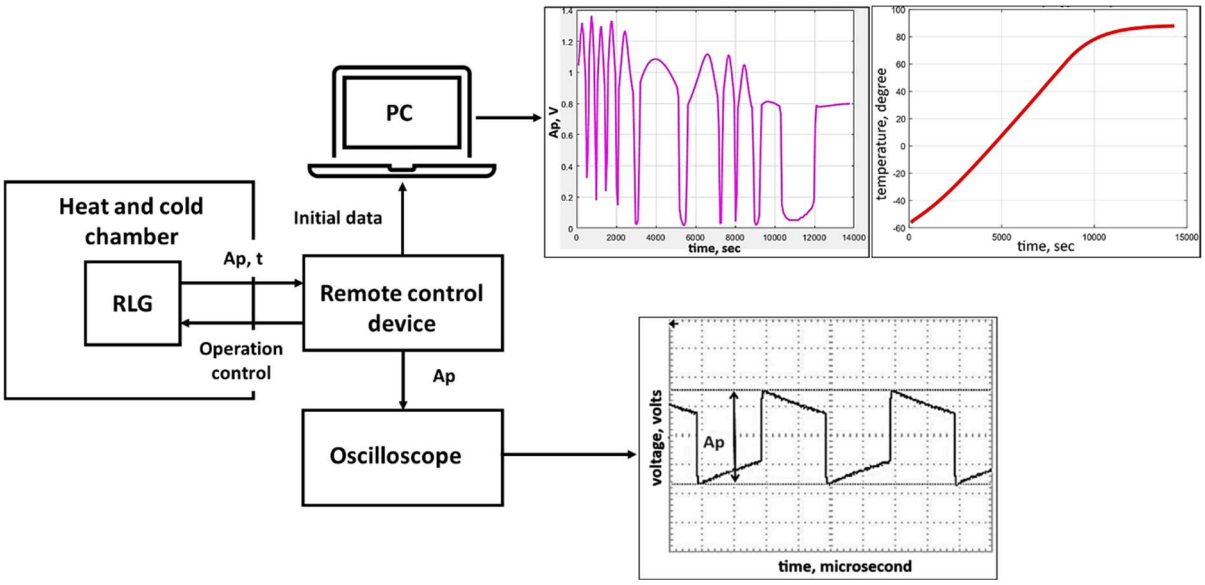

Fig. 2.1. Experimental study and initial data

It shows the dependence of the amplitude of the cavity detuning signal with an non-working CCS. At a linearly changing temperature *T* in the range from –55°C to 75°C at a rate of 1°/min inside the Heat and Cold Chamber, this characteristic reflects the sequential rearrangement of the RLG frequency spectrum relative to the center of the amplification circuit, caused by the cavity temperature deformation ΔL, nm.

It is known from paper that the typical value of the path length drift ΔL for Zeeman RLG type *ZLK*-16 in the operating temperature range is 3λ-4λ (from 1900 to 2500 nm) and may depend on many factors: TEC of glass-ceramic *SO*-115*M* and other structural elements, the length of the cavity, the method of pumping the active medium, the magnitude of the working

current of the discharge, and other factors [33,34]. Thus, having the time dependences of the signal *Ap* on temperature *T* as initial data, it becomes possible to create a model of the cavity temperature drift using a software method.

3. MATHLAB SIMULATION

To build the model, a special algorithm was developed, which was implemented in the MATLAB environment. Figure 3.1 shows a block diagram of the modeling of ring laser cavity temperature deformations algorithm.

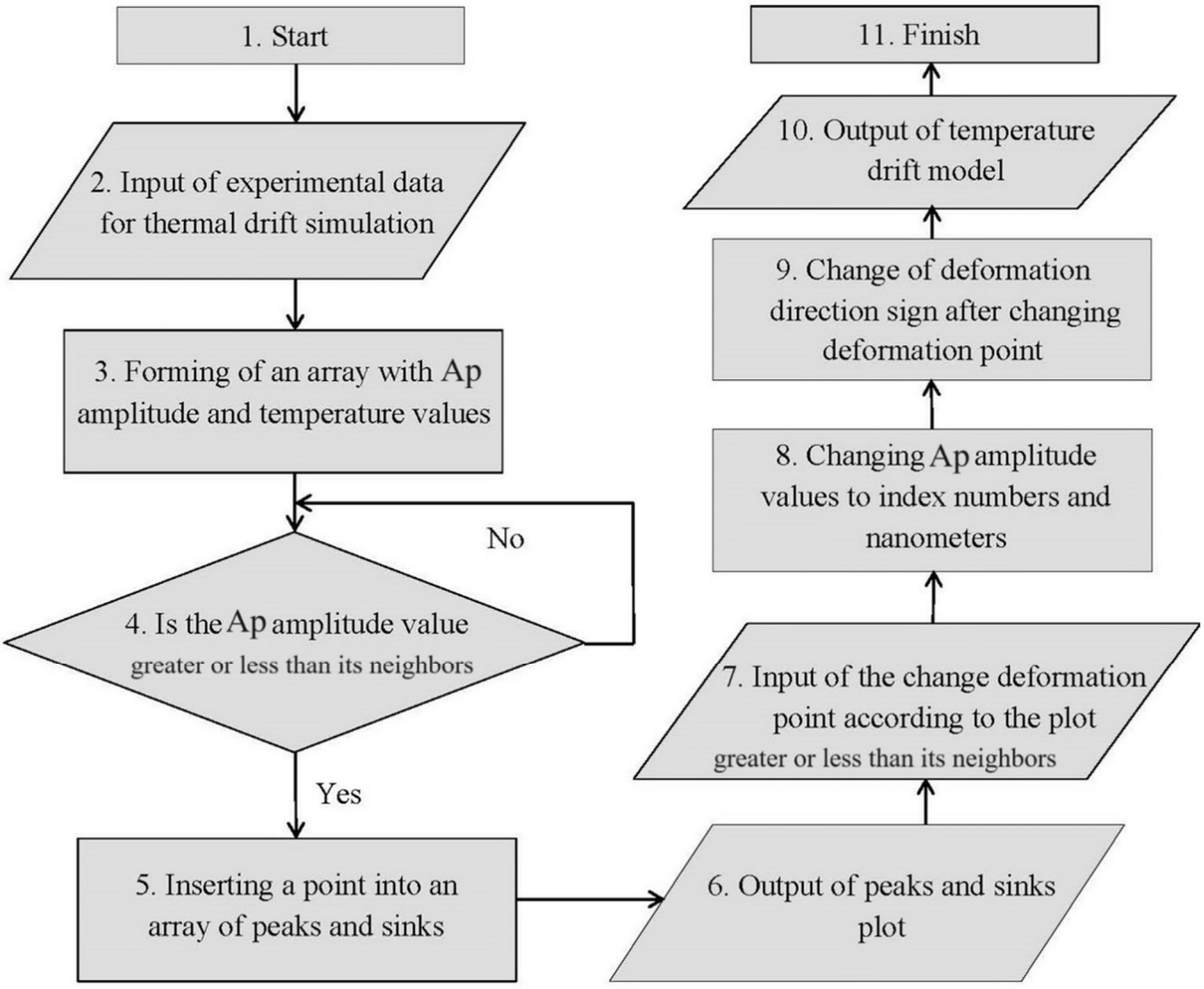

Fig. 3.1. Block diagram of the algorithm

Data from the text file WORK.txt obtained during the experimental study is written to the array "*A*" (3.1):

$$A=dlmread('WORK.txt') \tag{3.1}$$

In the array "*t*" the 3rd column of the array "*A*" is written, containing the readings of the temperature sensor. The 2nd column of the array "*A*" is written to the "*e*" array, containing the amplitude values of the detuning signal (3.2):

$$\begin{aligned} t&=A(:,3)\\ e&=A(:,2) \end{aligned} \tag{3.2}$$

The first empty intermediate arrays "*e1*" and "*t1*" are filled with values from the inflection point search algorithm. Next, the search for points of the array "*e*", the values of which are

greater or less than the values of their previous and subsequent points, which are entered into the intermediate array, also giving these points the values of the array "*t*" (3.3):

```
e1=[]
t1=[]
indx=1
for i = 2:size(e)-1
if ( ( e(i-1)< e(i))&& ( e(i+1)< e(i)))||( ( e(i-1) > e(i) ) && ( e(i+1)> e(i) ) );
e1(indx) = e(i);
t1(indx) =t(i);
indx = indx + 1;
end
```
(3.3)

After that, the values of the "*e1*" array are replaced by their corresponding serial numbers and converted to nanometers (3.4):

```
e1=1:size(e1');
e1=633*0.25*e1
```
(3.4)

Figure 3.2 shows an intermediate graph of the dependence of the signal *Ap* on temperature *T*, containing the key points of "peaks" and "dips" necessary to build the final model of the temperature deformation of the RLG cavity.

On the intermediate graph (Fig. 3.1) the number of the inflection point "*ind*" is selected, namely the number 9. This is the point at which the phase of the signal *Ap* changes.

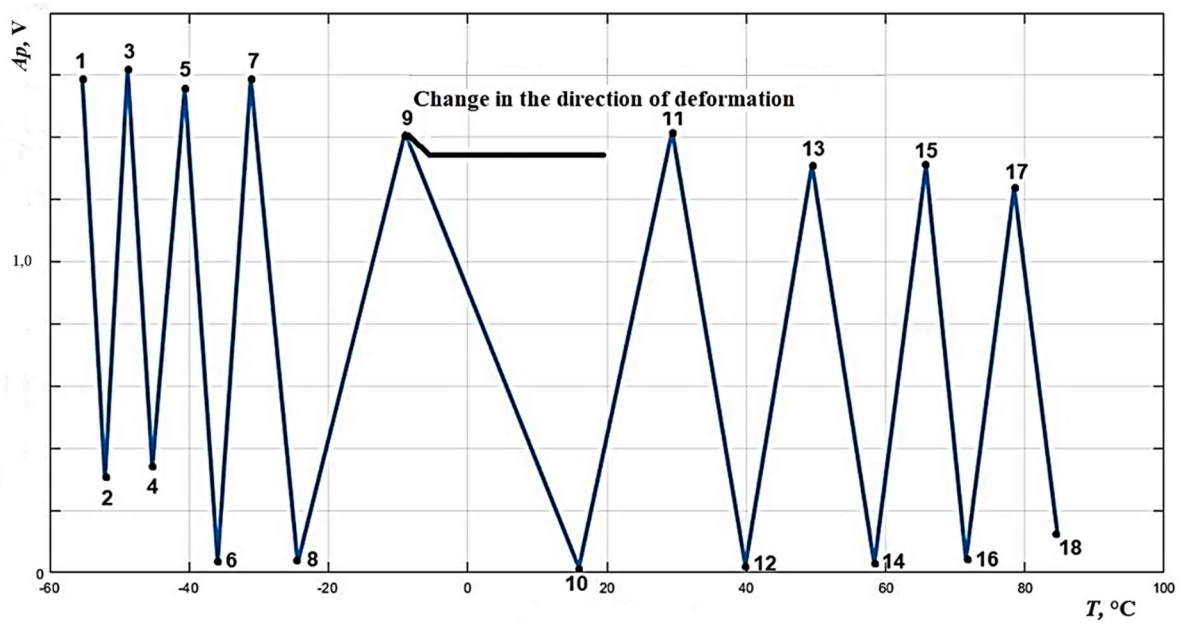

Fig. 3.2. Intermediate chart corresponding to the step of determining the Extremes of the cavity signal amplitude

From the values of the points of the "*e1*" array, the value of the magnitude of the amplitude change at the point of change in the direction of deformation is subtracted, which allows you to move the graph to zero coordinates at the inflection point (3.5):

```
ind=9
```
(3.5)


```
ind=9 e1=e1-e1(ind)
```

Next, the values "*e1*" and "*t1*" from the cycle are entered into the empty intermediate arrays "*ex*" and "*te*", which reflects the values of the change up to the inflection point relative to the abscissa axis (3.6):

```
ex=[]
te=[]
i1=1
for k=1:size(e1')
if k<ind
ex(i1)=-e1(k)'
te(i1)=t1(k)'
i1=i1+1
end
if k>=ind
ex(i1)=e1(k)'
te(i1)=t1(k)'
i1=i1+1
end
```

(3.6)

Based on the values from the "*ex*" and "*te*" arrays, a final graph of the dependence of the absolute change in the perimeter ΔL on temperature t is constructed. Figure 3.3 shows the temperature deformation model of the RLG resonator obtained in the MATLAB environment, which reflects the dependence of the absolute temperature change in the path length.

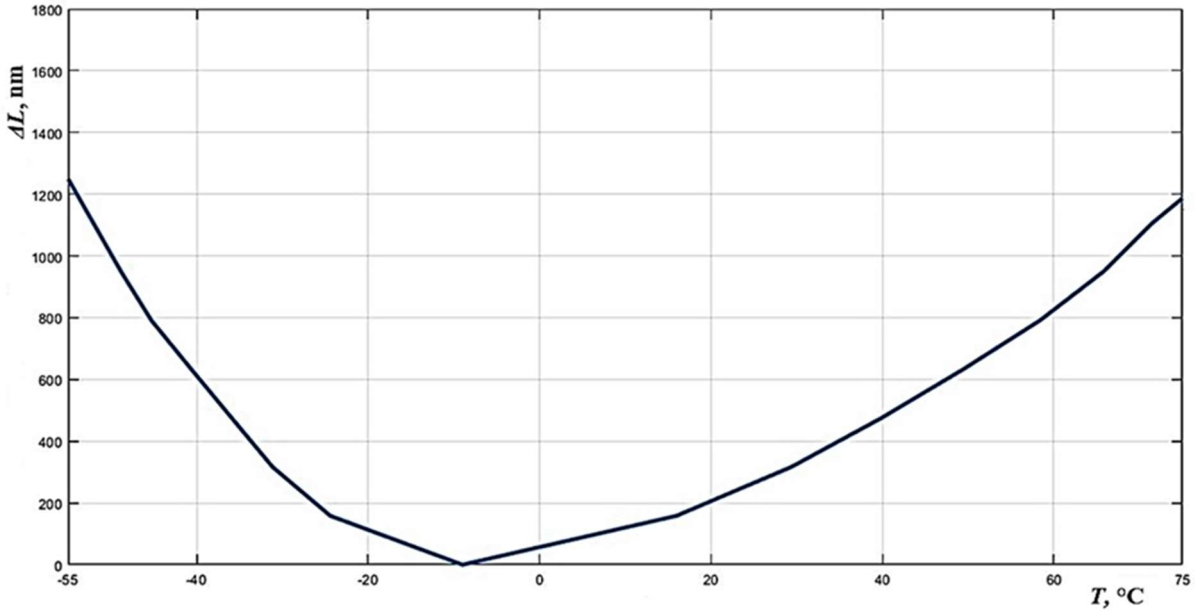

Fig. 3.3. Model of the ring laser cavity temperature drift

Having an idea about the nature of the path length temperature drift, it becomes possible to estimate the contribution of all structural elements of the RLG, which has TEC different from the glass-ceramic *SO*-115*M*, to the resulting temperature deformation of its cavity ΔL.

4. DISCUSSION OF THE RESULTS

Based on the initial data and thanks to the algorithm implemented in the MATLAB environment, it becomes possible to simulate and obtain the form of the dependence of the cavity temperature deformations at different stages of the RLG assembly, which will be described by expression (4.1):

$$\Delta L(T)=a\cdot T^3+ b\cdot T^2+c\cdot T+ d \tag{4.1}$$

where, ΔL is the value of thermal deformation, nm; T is the temperature value, °C; a, b, c, d are the polynomial coefficients determined by the design parameters of the RLG. In the present model (4.1), the coefficient a characterizes the nonlinear TEC of the glass-ceramic *SO*-115*M* in temperature range from –55°C to 75°C. The coefficient b takes into account the contribution of piezo actuators and c determines the influence to other RLG structural elements.

Figure 4.1 (Approximation of the ring laser cavity temperature drift) presents a graph of an approximating function of the type and its formula obtained using Microsoft Excel.

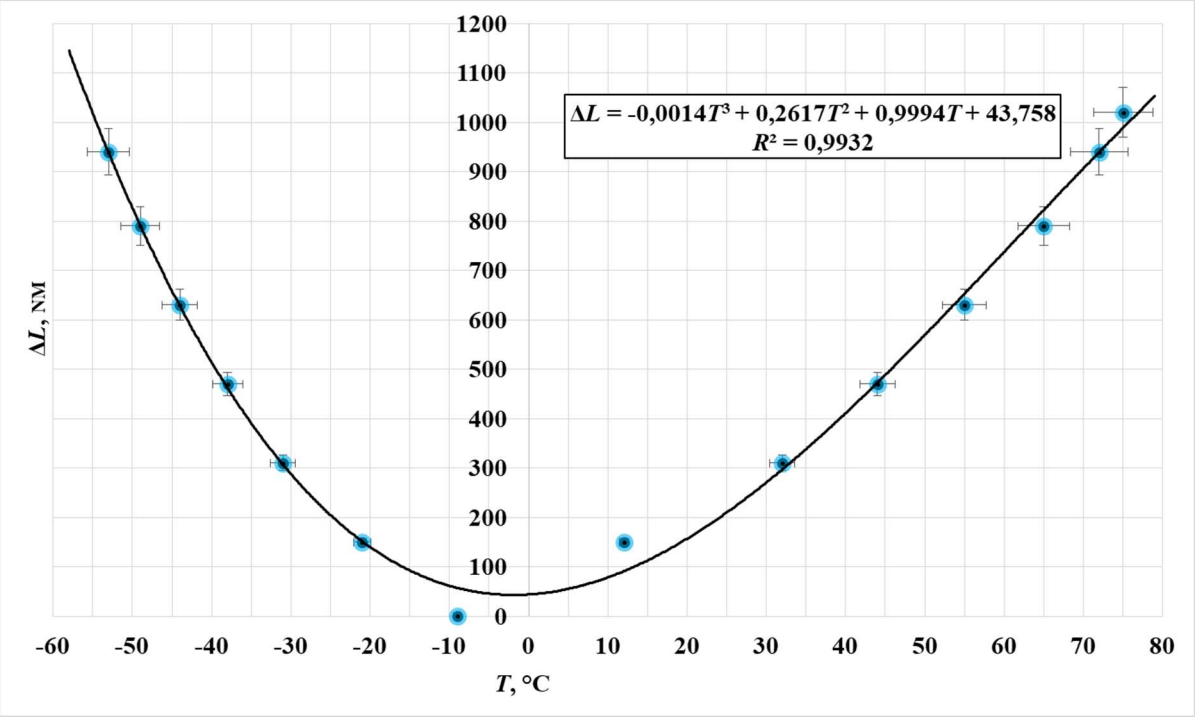

Fig 4.1. Approximation of the ring laser cavity temperature drift

It has a confidence level R=0,9932, which indicates the reliability of the obtained functional dependence. This opens up the possibility of using formula (4.1) to calculate the RLG cavity drift in the operating temperature range of the spacecraft, as well as to use it as a governing law for the CCS active stabilization (4.2).

$$U_{ccs}(t) =U_p\cdot\Delta L(T(t)) \tag{4.2}$$

where, U_{ccs} is the CCS control voltage, V; t is the operating time, sec, °C; U_p·is the piezo actuators transmission coefficient, V/nm.

5. CONCLUSION

The presented mathematical model demonstrates the behavior of the temperature deformation of the RLG cavity at different stages of its generation. When adding new structural elements, a shift of the inflection point and a change in the resulting cavity deformation are observed.

This makes it possible to estimate the contribution of each structural element to the resulting thermal deformation of the ring laser cavity. The next step in this work will be to check the operability of the approximating function as the governing law of the active CCS.

The proposed methodology not only addresses the critical challenge of RLG thermal compensation but also contributes to the advancement of fully autonomous navigation systems [35] for next-generation spacecraft – from Earth observation satellites to interplanetary probes. Further efforts will focus on implementing the model in industrial-grade gyroscopes for launch vehicles and crewed missions.

REFERENCES

1. Hering, E., Schönfelder, G., Basler, S., Biehl, K-E., Burkhardt, T. et. al. (2022). Geometric Quantities. In Hering E., Schönfelder G. (Eds.). *Sensors in Science and Technology* (pp.147–372). Springer, Wiesbaden, https://doi.org/10.1007/978-3-658-34920-2_3
2. Logashina, I. V., Chumachenko, E. N., Bober, S. A., Aksenov, S. A. (2009). Thermal stress state of a laser-gyroscope housing for use in space. *Russian Engineering Research*, 29, 751–755, https://doi.org/10.3103/S1068798X09080012
3. Dell'Olio, F., Natale, T., Wang, Y. C., & Hung, Y. J. (2023). Miniaturization of Interferometric Optical Gyroscopes: A Review. *IEEE Sensors Journal*, **23**(24), 29948–29968, doi: 10.1109/JSEN.2023.3327217
4. Sinelnikov, A.O., Tikhmenev, N.V., Ushanov, A.A., Medvedev, V.M. (2024). State-of-the-Art and Development Trends of Inertial Navigation Systems Based on the Ring laser Gyroscopes. *Photonics Russia*, **18**(6), 450–466, doi: 10.22184/1993-7296.FRos.2024.18.6.450.466
5. *Ring Laser Gyroscope Market Report: Trends, Forecast and Competitive Analysis to 2030*, [Online]. Available: https://www.researchandmarkets.com/reports/5928625/ring-laser-gyroscope-market-report-trends#rela4–5030627.
6. Corke, P. (2022). Navigation. In: Robotics and Control. *Springer Tracts in Advanced Robotics*, **141**, (pp. 123–147). Springer, Cham, doi: 10.1007/978-3-030-79179-7_5
7. Chopra, K. N. (2021). Ring Laser Gyroscopes. *In: Optoelectronic Gyroscopes. Progress in Optical Science and Photonics*, **11**, Springer, Singapore, doi: 10.1007/978-981-15-8380-3_1
8. Robin, L. & Perlmutter, M. (2012). Gyroscopes and IMUs for De-fence Aerospace and Industrial. *Report by Yole development*.
9. Damianos, D. & Girardin, G. (2020). High-End Inertial Sensors for Defense, Aerospace & Industrial Applications. *Market and Technology Report by Yole development*.
10. Oelschlaeger, M. & Thielman, L. O. (1990). GG1308 ring laser gyro inertial measurement systems: Honeywell's low-cost solution for tactical applications. *Proc. of IEEE Position Location and Navigation Symposium* (Las Vegas, NV), 528–536.
11. Fang, F., Wenhui, Z., & Zilong, L. (2022) Coupled Dynamic Analysis and Decoupling Optimization Method of the Laser Gyro Inertial Measurement Unit. *Sensors*, **20**, 111, doi: 10.3390/s20010111
12. Aronowitz, F. (1999). Fundamentals of the ring laser gyro, 3-1-3-45. *Optical Gyros and their Application*, RTO AGARDograph 339.
13. Azarova, V. V., Golyaev, Yu. D. & Savelyev, I. I. (2015). Zeeman laser gyroscopes. *Quantum Electronics,* **45**(2), 171–179.
14. Sinelnikov, A. O., Tikhmenev, N. V., Ushanov, A. A. & Nazarov, S. I. (2023). Interaction of the Dither of a Ring Laser Gyroscope with an External Mechanical Disturbance. *IEEE Xplore*, 1–4, doi: 10.23919/ICINS51816.2023.10168376
15. Kuznetsov, E., Golyaev, Y., Kolbas, Y., Kofanov, Y., et. al. (2020). The method of intelligent computer simulation of laser gyros behavior under vibrations to ensure their

reliability and cost-effective development and production. *Proc. of SPIE*, 11523, 115230B.
16. Sinel'nikov, A. O., Medvedev, A. A., Golyaev, Y. D., Grushin, M. E., & Chekalov, D. I. (2021). Thermal Zero Drifts in Magneto-Optical Zeeman Laser. *Gyroscopy and Navigation,* **129**(4), 308–313, doi: 10.1134/S2075108721040076
17. Wu, F., Zhang, M-H., Fu, X., Guo, X., Wang, J-L., et. al. (2017). Design of a laser frequency stabilization system for space three-axis mechanical dithering laser gyro. *Zhongguo Guanxing Jishu Xuebao,* **25**(2), 265–268.
18. Khokhlov, I. N., Sinelnikov, A. O. & Fetisova, N. E. (2022). Scale Factor Correction Model for Zeeman Laser Gyroscopes. *Proc. of 29th St. Petersburg International Conference on Integrated Navigation Systems (ICINS)* (Saint Petersburg, Russia), 1–4, doi: 10.23919/ICINS51784.2022.9815382
19. Soloveva, T., Sinelnikov, A., Kuznetsov, E., Golyaev, Y. & Kolbas, Y. (2022). Computer simulation of processes in the resonator length control system of the Zeeman laser gyro. *Proc. of International Conference on Optoelectronic Information and Computer Engineering (OICE 2022)*, (Kunming, Yunnan, China), 123080B, doi: 10.1117/12.2645990
20. Venkateswaran, C, Sreemoolanadhan, H. & Vaish, R. (2022). Lithium aluminosilicate (LAS) glass-ceramics: a review of recent progress. *International Materials Reviews*, **67**(6), 620–657, doi: 10.1080/09506608.2021.1994108
21. Naumov, A. S. & Sigaev, V. N. (2024). Transparent Lithium-Aluminum-Silicate Glass-Ceramics (Overview). *Glass Ceram.*, **80**, 491–499, doi: 10.1007/s10717-024-00639-4
22. Mitra, I. (2022). ZERODUR: a glass-ceramic material enabling optical technologies. *Optical Materials Express*, **12**(9), 3563–3576, doi: 10.1364/OME.460265
23. Naumov, A. S., Shakhgildyan, G. Y., Golubev, N. V., et. al. (2024). Tuning the Coefficient of Thermal Expansion of Transparent Lithium Aluminosilicate Glass-Ceramics by a Two-Stage Heat Treatment. *Ceramics*, **7**, 1–14, doi: 10.3390/ceramics7010001
24. Sinelnikov, A. O., Zapotylko, N. R., Zubarev, Y. A., et. al. (2023). Aspects of Sitall SO-115M Use in the Fabrication of the Optical Components of He–Ne Ring Lasers. *Glass Ceram*, **80**, 171–177, https://doi.org/10.1007/s10717-023-00579-5
25. Kuznetsov, E., Golyaev, Yu., Kolbas, Yu., Kofanov, Yu., Kuznetsov, N., et. al. (2021). Thermal computer modeling of laser gyros at the design stage: a promising way to improve their quality and increase the economic efficiency of their development and production. *Optical and Quantum Electronics*, **53**(10), 596, 1–15.
26. Filatov, Y. D., Sidorko, V. I., Kovalev, S. V. & Kovalev, V. A. (2021). Effect of the Rheological Properties of a Dispersed System on the Polishing Indicators of Optical Glass and Glass Ceramics. *Journal of Superhard Materials*, **43**, 65–73, doi: 10.3103/S1063457621010032
27. Weng, J., Bian, X., Kou, K. & Lian, T. (2020) Optimization of Ring Laser Gyroscope Bias Compensation Algorithm in Variable Temperature Environment. *Sensors*, **20**(2), 377, doi: 10.3390/s20020377
28. Liang, H., Ren, Q., Zhang, D., Zhao, X. & Guo, Y. (2022). The Temperature Compensation Method for the Laser Gyro Based on the Relevance Vector Machine. In Jia Y., Zhang W., Fu Y., Yu Z., Zheng S. (Eds). *Proceedings of 2021 Chinese Intelligent Systems Conference. Lecture Notes in Electrical Engineering*. Springer, Singapore, 803, 367–375, doi: 10.1007/978-981-16-6328-4_39
29. Li, Y., Fu, L., Wang, L., He, L. & Li, D. (2022). Laser Gyro Temperature Error Compensation Method Based on NARX Neural Network Embedded into Extended Kalman Filter. In: Yan L., Duan H., Yu X. (Eds.). *Advances in Guidance, Navigation*

and Control. Lecture Notes in Electrical Engineering (pp. 3309–3320). Springer, Singapore, 644.

30. Kolbas, Y. Y., Pyatnitskii, Y. S., Rodionov, M. I. & Saveliev, I. I. (2022). Output characteristic of four-frequency Zeeman laser gyroscope with an alternating frequency bias. *Quantum Electronics*, **52**(2), 202–206, doi: 10.1070/QEL17991
31. Varenik, A. I., Gorshkov, V. N., Grushin, M .E., Ivanov, M. A. Kolbas, Yu. Yu., et. al. (2021). Digital system for frequency regulation and stabilization of a four-frequency Zeeman laser gyroscope. *Quantum Electron*, **51**(3), 276–282.
32. Zubarev, Y. A., Sinelnikov, A. O. & Fetisova, N. E. (2022). A study of the Temperature Stability of the Zeeman Laser Gyro Ring Resonator. *Proc. of 29th Saint Petersburg International Conference on Integrated Navigation Systems (ICINS)* (St. Petersburg, Russia), 1–4, doi: 10.23919/ICINS51784.2022.9815336
33. Li, Z., Zhang, L. & Wu, K. (2023). Filter design for laser inertial navigation system based on improved pigeon-inspired optimization. *Aerospace*, **10**(63), doi: 10.3390/aerospace10010063
34. Sinelnikov, A. O., Zubarev, Y. A. & Tereshenko D. A. (2023). Rapid Persistence Testing of Ring Laser Gyroscopes. *Proc. of 30th Saint Petersburg International Conference on Integrated Navigation Systems (ICINS)* (St. Petersburg, Russia), 1–3, doi: 10.23919/ICINS51816.2023.10168522
35. Peshekhonov, V. G. (2022) High-Precision Navigation Independently of Global Navigation Satellite Systems Data. *Gyroscopy Navig.*, **13**, 1–6, 2022, doi: 10.1134/S2075108722010059

